Radiation Effect on MHD Stagnation-Point Flow of a Nanofluid over an Exponentially Stretching Sheet

Imran ANWAR[1,2], Sharidan SHAFIE[1,*] and Mohd Zuki SALLEH[3]

[1]*Department of Mathematical Sciences, Faculty of Science, Universiti Teknologi Malaysia, Johor, Malaysia*
[2]*Department of Mathematics, Faculty of Science, University of Sargodha, Pakistan*
[3]*Faculty of Industrial Science and Technology, Universiti Malaysia Pahang, Pahang, Malaysia*

([*]**Corresponding author's e-mail: ridafie@yahoo.com**)

Abstract

This paper theoretically investigates the radiation effect on magnetohydrodynamics (MHD) stagnation-point flow of a nanofluid over an exponentially stretching sheet under the assumptions of a small magnetic Reynolds number. The sheet is stretched with an exponential velocity in the presence of a non-uniform magnetic field **B** applied in a transverse direction normal to the flow. By using the modified Bernoulli's equation, a highly nonlinear nanofluid problem is modeled for an electrically conducting nanofluid. The momentum, thermal and concentration boundary layer thicknesses are intensified for the incorporated flow parameters such as Brownian motion parameter Nb, thermophoresis parameter Nt, Prandtl number Pr, Lewis number Le, Hartmann number M_{exp} and velocity ratio parameter ε. Also by an appropriate similarity transformation, the system of nonlinear partial differential equations is reduced to ordinary differential equations. These equations subjected to the boundary conditions are solved numerically using the Keller-box method. Numerical results are plotted and discussed for pertinent flow parameters. A comparison with existing results in the literature is also provided.

Keywords: MHD, radiation effect, stagnation-point flow, numerical solution.

Introduction

During the last few decades, stagnation-point flow has engaged the attention of many researchers due to its growing applications in industry such as cooling of electronic devices by fans, cooling of nuclear reactors during emergency shutdown and hydrodynamic processes. In fluid mechanics, a point where the local velocity of the fluid becomes zero is called a stagnation-point. This point marks a location in the flow where the approaching flow divides to pass on both sides along the surface. The stagnation-point exists everywhere in the sense that certainly appears as a component of more complicated flow fields. For example, in some situations, flow is stagnated by a solid wall while in others; there is a line interior to a homogeneous fluid domain or the interface between 2 immiscible fluids [1-3]. The stagnation-point flow towards a stretching or shrinking sheet has drawn considerable attention of several researchers and a good amount of literature has been generated on this topic [4-12].

In all the above investigations the stagnation-point flow is studied for traditional viscous fluids. However, during the last few decades, the developments in the field of nanotechnology based on a special class of fluids called nanofluids have become an extensive area of research due to its growing applications in many engineering and technological processes. Hence, this is the motivation behind the choice of the present study. More exactly, the current article deals with the stagnation-point flow of a nanofluid over an exponentially stretching sheet. Although, the presence of additional nonlinear terms in the equations of motion make it more complex and subtle as compared to other fluid models [13-15].

However, researchers are getting interested in studying the boundary layer flow of nanofluids with different physical aspects.

The conjugate effects of heat and mass transfer [16,17] on magnetic nanoparticles experience a force induced by an electric current which results for the modification in fluid motions. This electrically conducting nanofluid interacts with a transverse magnetic field which induces Lorentz forces. More importantly, the study of the magnetohydrodynamics (MHD) stagnation-point flow of nanofluid over a continuously stretching surface has attracted considerable attention due to its numerous applications in industrial manufacturing processes. This effect is used for the cooling purposes in nuclear reactors where liquid sodium is used for the induction flow meter which depends on the potential differences in the flow [18]. On the other hand, the radiation effect is quite significant in many engineering processes at high temperature and is also important for the design of pertinent equipment [19,20]. As electrically conducting fluid has important applications in nuclear reactors cooling systems, biomedicine, electronics, glass fiber, hot rolling, food and transportation [21], the present study aims for the radiation effect on MHD stagnation-point flow of a nanofluid over an exponentially stretching sheet.

Problem formulation

Consider a steady two-dimensional boundary layer stagnation-point flow of a nanofluid over an exponentially stretching sheet. The stretching and free stream velocities are assumed to be of the forms $u_w(x) = ae^{(x/l)}$ and $u_\infty(x) = be^{(x/l)}$ respectively, where a and b are constants, x is the coordinate measured along the stretching surface and l is the length of the sheet. A non-uniform transverse magnetic field of strength $B(x) = B_0 \, e^{(x/2l)}$ is imposed parallel to the $y-$axis (normal to the flow direction), where B_0 is the uniform magnetic field strength. It is assumed that the induced magnetic field due to the motion of an electrically conducting fluid is negligible. Further, it is also assumed that the external electrical field is zero and the electric field due to the polarization of charges is negligible [22]. **Figure 1** shows that the temperature T and the nanoparticles fraction C take forms $T_w(x)$ and $C_w(x)$, respectively, whereas the ambient values of temperature T_∞ and the nanoparticles fraction C_∞ are attained as y tends to infinity.
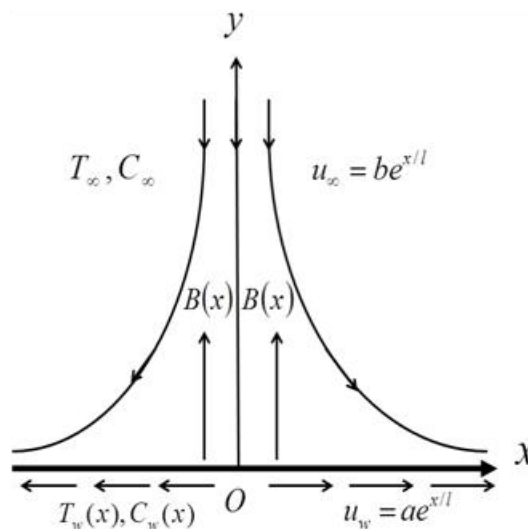
Figure 1 Physical model and coordinate system.

The governing boundary layer equations based on the balance laws of momentum, energy and concentration in nanofluid problems are as follows;

$$\frac{\partial u}{\partial x} + \frac{\partial v}{\partial y} = 0 ,$$ (1)

$$u \frac{\partial u}{\partial x} + v \frac{\partial u}{\partial y} = u_\infty \frac{du_\infty}{dx} + \frac{\mu}{\rho_f} \frac{\partial^2 u}{\partial y^2} + \frac{\sigma B^2(x)}{\rho_f} [u_\infty - u],$$ (2)

$$u \frac{\partial T}{\partial x} + v \frac{\partial T}{\partial y} = \alpha \frac{\partial^2 T}{\partial y^2} - \frac{1}{(\rho c)_f} \frac{\partial q_r}{\partial y} + \tau \left[D_B \frac{\partial C}{\partial y} \frac{\partial T}{\partial y} + \frac{D_T}{T_\infty} \left(\frac{\partial T}{\partial y} \right)^2 \right],$$ (3)

$$u \frac{\partial C}{\partial x} + v \frac{\partial C}{\partial y} = D_B \frac{\partial^2 C}{\partial y^2} + \frac{D_T}{T_\infty} \frac{\partial^2 T}{\partial y^2} .$$ (4)

Here u and v are the velocity components in the x and y-directions respectively, μ is the viscosity, ρ_f is the density of the base fluid, σ is the electrical conductivity, $B(x)$ is the magnetic field, $\alpha = \frac{k}{(\rho c)_f}$ where k is the thermal conductivity and $(\rho c)_f$ is the heat capacitance of the base fluid, $\tau = \frac{(\rho c)_p}{(\rho c)_f}$ where $(\rho c)_p$ is the heat capacitance of the nanoparticles, D_B is the Brownian diffusion coefficient, D_T is the thermophoresis diffusion coefficient and q_r is the radiation flux. The Rosseland approximation is defined as [23,24];

$$q_r = -\frac{4\sigma^*}{3k^*} \frac{\partial T^4}{\partial y},$$ (5)

where σ^* is the Stefan-Boltzmann constant and k^* is the mean absorption coefficient. It is assumed that the temperature difference between the free stream T_∞ and local temperature T is small enough, expanding T^4 in a Taylor series about T_∞ and neglecting higher order terms results for;

$$T^4 \cong 4T_\infty^3 T - 3T_\infty^4 .$$ (6)

After substituting Eqs. (5) and (6), Eq. (3) reduces to;

$$u \frac{\partial T}{\partial x} + v \frac{\partial T}{\partial y} = \left(\alpha + \frac{16\sigma^* T_\infty^3}{3k^* (\rho c)_f} \right) \frac{\partial^2 T}{\partial y^2} + \tau \left[D_B \frac{\partial C}{\partial y} \frac{\partial T}{\partial y} + \frac{D_T}{T_\infty} \left(\frac{\partial T}{\partial y} \right)^2 \right].$$ (7)

The subjected boundary conditions are;

$$u = u_w(x) = ae^{(x/l)}, \ v = 0, \ T = T_w(x), \ C = C_w(x), \quad \text{at} \quad y = 0,$$

$$u \to u_\infty(x) = be^{(x/l)}, \ v \to 0, \ T \to T_\infty, \ C \to C_\infty, \quad \text{as} \quad y \to \infty. \tag{8}$$

The prescribed temperature and the concentration on the surface of the sheet are assumed of the forms $T_w(x) = T_\infty + T_0 e^{(x/2l)}$ and $C_w(x) = C_\infty + C_0 e^{(x/2l)}$, where T_0, C_0 are the reference temperature and concentration respectively. Now, the nonlinear partial differential equations are reduced into nonlinear ordinary differential equations. For that purpose, a stream function $\psi = \psi(x, y)$ is defined as;

$$u = \frac{\partial \psi}{\partial y}, \ v = -\frac{\partial \psi}{\partial x}, \tag{9}$$

where, the continuity Eq. (1) is satisfied identically. The similarity transformation is defined as [20];

$$\psi = \sqrt{2l\nu a}\,e^{(x/2l)} f(\eta), \ \theta(\eta) = \frac{T - T_\infty}{T_w - T_\infty},$$

$$\phi(\eta) = \frac{C - C_\infty}{C_w - C_\infty}, \ \eta = y\sqrt{a/2\nu l}\,e^{(x/2l)}. \tag{10}$$

On substituting Eq. (10), Eqs. (2), (4) and (7) reduce to the following system of nonlinear ordinary differential equations.

$$f''' + ff'' - 2f'^2 + 2\varepsilon^2 - M_{\exp}(f' - \varepsilon) = 0, \tag{11}$$

$$\Pr_N \theta'' + f\theta' - f'\theta + Nb\phi'\theta' + Nt\theta'^2 = 0, \tag{12}$$

$$\phi'' + Lef\phi' - Lef'\phi + Nt_b\theta'' = 0, \tag{13}$$

where

$$\varepsilon = \frac{b}{a}, \ \nu = \frac{\mu}{\rho_f}, \ \Pr = \frac{\nu}{\alpha}, \ Le = \frac{\nu}{D_B}, \ M_{\exp} = \frac{2l\sigma B_0^2}{a\rho_f}$$

$$Nb = \frac{\tau D_B(C_w - C_\infty)}{\nu}, \ Nt = \frac{\tau D_T(T_w - T_\infty)}{\nu T_\infty}. \tag{14}$$

Here, prime denote the differentiation with respect to η, ε is the velocity ratio parameter, ν is the

kinematic viscosity of the fluid, Pr is the Prandtl number, Le is the Lewis number, $M_{\exp}$ is the Hartmann number, $\mathrm{Pr}_N = \dfrac{1}{\mathrm{Pr}}(1 + \dfrac{4}{3}N)$ where $N = \dfrac{4\sigma^* T_\infty^3}{\alpha k^*}$ is the radiation parameter, $Nt_b = \dfrac{Nt}{Nb}$ where Nb is the Brownian motion parameter and Nt is the thermophoresis parameter. The corresponding boundary conditions (8) are transformed into;

$$f(\eta) = 0, \; f'(\eta) = 1, \; \theta(\eta) = 1, \; \phi(\eta) = 1 \; \text{ at } \; \eta = 0,$$

$$f'(\eta) \to \varepsilon, \; \theta(\eta) \to 0, \; \phi(\eta) \to 0 \; \text{ as } \; \eta \to \infty. \tag{15}$$

The parameters of practical interest in the formulated problem are velocity, heat and mass transfer respectively, which are presented in terms of skin-friction C_f, Nusselt number Nu and Sherwood number Sh. Using the transformed variables (10), the non-dimensional expressions for the skin-friction coefficient $C_{fx}(0) = f''(0)$, the reduced Nusselt number $-\theta'(0)$ and the reduced Sherwood number $-\phi'(0)$ respectively are defined as;

$$C_{fx}(0) = C_f \sqrt{(2l/x)\mathrm{Re}_x}, \; -\theta'(0) = \frac{Nu}{\left(1 + \dfrac{4}{3}N\right)\sqrt{(x/2l)\mathrm{Re}_x}}, \; -\phi'(0) = \frac{Sh}{\sqrt{(x/2l)\mathrm{Re}_x}}, \tag{16}$$

where, $\mathrm{Re}_x = u_w(x)x/\nu$ is the local Reynolds number based on the stretching velocity. The transformed nonlinear ordinary differential Eqs. (11) - (13) subjected to the boundary conditions (15) are solved numerically by using the Keller-box method [25].

Numerical procedure for Keller-box method

In the following section, the numerical procedure of the Keller-box method for the radiation effect on MHD stagnation-point flow of a nanofluid over an exponentially stretching sheet is explained. This method is very simple and highly accurate in computing results for the boundary layer flow problems. Therefore, Eqs. (11) - (13) subject to the boundary conditions (15) have been solved numerically using the Keller-box method for the finite difference method, Newton's method, the block-elimination method and starting conditions.

The finite difference method

Eqs. (11) - (13) subject to the boundary conditions (15) are written in a system of first order differential equations [25]. For this purpose, new dependent variables are introduced for $f(\eta)$, $u(\eta)$, $v(\eta)$, $g(\eta)$, $p(\eta)$, $q(\eta)$, and $s(\eta)$. Also, $\theta(\eta)$ and $\phi(\eta)$ are replaced with $g(\eta)$ and $q(\eta)$ respectively that represent the fluid temperature and concentration respectively. Therefore, the first-order equations are;

$$\begin{aligned}
&f'(\eta) = u(\eta), \; u'(\eta) = v(\eta), \; g'(\eta) = p(\eta), \; q'(\eta) = s(\eta), \\
&v' + fv - 2u^2 + M_{\exp}(\varepsilon - u) + 2\varepsilon^2 = 0, \\
&\mathrm{Pr}_N \; p' + fp - ug + Nbsp + Ntp^2 = 0, \\
&s' + Le(fs - uq) + Nt_b p' = 0.
\end{aligned} \tag{17}$$

The boundary conditions in terms of new dependent variable η, become;

$$f(\eta) = 0, \ u(\eta) = 1, \ g(\eta) = 1, \ q(\eta) = 1 \qquad \text{at} \qquad \eta = 0,$$
$$u(\eta) \rightarrow \varepsilon, \ g(\eta) \rightarrow 0, \ q(\eta) \rightarrow 0 \qquad \text{as} \qquad \eta \rightarrow \infty. \qquad (18)$$

The net rectangle is considered in the *x-η* plane as shown in **Figure 2** and the net points are defined as below;

$$x^0 = 0, \qquad x^i = x^{i-1} + k_i, \quad i = 1, 2, 3, \ ...... \ I, \qquad (19)$$

$$\eta_0 = 0, \qquad \eta_j = \eta_{j-1} + h_j \qquad j = 1, 2, 3, \ ...... \ J, \quad \eta_J \equiv \eta_\infty, \qquad (20)$$

where k_i is the Δx–spacing and h_j is the $\Delta \eta$–spacing. Here *i* and *j* are just a sequence of numbers that indicate the coordinate location, not tensor indices or exponents.
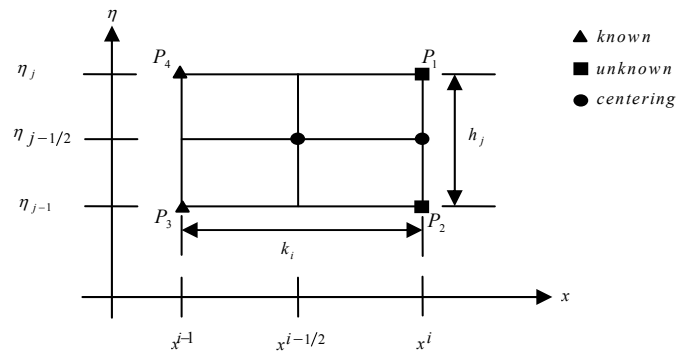
Figure 2 Net rectangle for difference approximations.

The derivatives in the *x*-direction are given by finite difference, for example;

$$\frac{\partial u}{\partial x} = \frac{u^i - u^{i-1}}{k_i}, \qquad (21)$$

while the derivatives in the *η*-direction are replaced by finite difference, for example;

$$v' = \frac{\partial v}{\partial \eta} = \frac{v_j - v_{j-1}}{h_j}, \qquad (22)$$

for any points;

$$()_j^{i-1/2} = \frac{1}{2}\left[()_j^i + ()_j^{i-1} \right], \qquad (23)$$

and

$$()_{j-1/2}^{i} = \frac{1}{2}\left[()_{j}^{i} + ()_{j-1}^{i}\right], \tag{24}$$

The difference equations, which are to approximate Eqs. (17), are written by considering one mesh rectangle as shown in **Figure 2**. Using centred-difference derivatives, the finite difference approximations of the ordinary differential Eqs. (17) are written for the midpoint ($\eta_{j-1/2}$) of the segment P_1P_2. This process is called "centring about ($\eta_{j-1/2}$)" written as;

$$\frac{\left(f_j^i - f_{j-1}^i\right)}{h_j} = \frac{1}{2}\left(u_j^i + u_{j-1}^i\right) = u_{j-1/2}^i, \quad \frac{\left(u_j^i - u_{j-1}^i\right)}{h_j} = \frac{1}{2}\left(v_j^i + v_{j-1}^i\right) = v_{j-1/2}^i,$$

$$\frac{\left(g_j^i - g_{j-1}^i\right)}{h_j} = \frac{1}{2}\left(p_j^i + p_{j-1}^i\right) = p_{j-1/2}^i, \quad \frac{\left(q_j^i - q_{j-1}^i\right)}{h_j} = \frac{1}{2}\left(s_j^i + s_{j-1}^i\right) = s_{j-1/2}^i,$$

$$\frac{\left(v_j^i - v_{j-1}^i\right)}{h_j} + \left[\left(\frac{f_j^i + f_{j-1}^i}{2}\right)\left(\frac{v_j^i + v_{j-1}^i}{2}\right)\right] - \left[2\left(\frac{u_j^i + u_{j-1}^i}{2}\right)^2\right]$$

$$+ + M_{exp}\left[\varepsilon - \left(\frac{u_j^i + u_{j-1}^i}{2}\right)\right] + 2\varepsilon^2 = 0,$$

$$Pr_N \frac{\left(p_j^i - p_{j-1}^i\right)}{h_j} + \left[\left(\frac{f_j^i + f_{j-1}^i}{2}\right)\left(\frac{p_j^i + p_{j-1}^i}{2}\right)\right] - \left[\left(\frac{u_j^i + u_{j-1}^i}{2}\right)\left(\frac{g_j^i + g_{j-1}^i}{2}\right)\right]$$

$$+ Nb\left[\left(\frac{s_j^i + s_{j-1}^i}{2}\right)\left(\frac{p_j^i + p_{j-1}^i}{2}\right)\right] + Nt\left[\left(\frac{p_j^i + p_{j-1}^i}{2}\right)^2\right] = 0,$$

$$\frac{\left(s_j^i - s_{j-1}^i\right)}{h_j} + Le\left[\left(\frac{f_j^i + f_{j-1}^i}{2}\right)\left(\frac{s_j^i + s_{j-1}^i}{2}\right) - \left(\frac{u_j^i + u_{j-1}^i}{2}\right)\left(\frac{q_j^i + q_{j-1}^i}{2}\right)\right] \tag{25}$$

$$+ Nt_b\left[\left(\frac{p_j^i - p_{j-1}^i}{h_j}\right)\right] = 0.$$

At $x = x^i$, the subjected boundary conditions (18) in terms of the dependent variable (η) become;

$$f_0^i = 0, \ u_0^i = 1, \ g_0^i = 1, \ q_0^i = 1,$$

$$u_J^i = \varepsilon, \ g_J^i = 0, \ q_J^i = 0. \tag{26}$$

Newton's method

If ($f_j^{i-1}, u_j^{i-1}, v_j^{i-1}, g_j^{i-1}, p_j^{i-1}, q_j^{i-1}, s_j^{i-1}$) are assumed to be known for $0 \le j \le J$, then the solution of the unknown ($f_j^i, u_j^i, v_j^i, g_j^i, p_j^i, q_j^i, s_j^i$) $0 \le j \le J$, have to be obtained. For simplicity of notations, unknown at $x = x^i$, ($f_j^i, u_j^i, v_j^i, g_j^i, p_j^i, q_j^i, s_j^i$) are written as ($f_j, u_j, v_j, g_j, p_j, q_j, s_j$). After multiplying with h_j, the system of Eqs. (25) can be written as;

$$f_j^i - f_{j-1}^i = \frac{h_j}{2}\left(u_j^i + u_{j-1}^i\right) = u_{j-1/2}^i, \quad u_j^i - u_{j-1}^i = \frac{h_j}{2}\left(v_j^i + v_{j-1}^i\right) = v_{j-1/2}^i,$$

$$g_j^i - g_{j-1}^i = \frac{h_j}{2}\left(p_j^i + p_{j-1}^i\right) = p_{j-1/2}^i, \quad q_j^i - q_{j-1}^i = \frac{h_j}{2}\left(s_j^i + s_{j-1}^i\right) = s_{j-1/2}^i,$$

$$v_j^i - v_{j-1}^i + h_j\left[\left(\frac{f_j^i + f_{j-1}^i}{2}\right)\left(\frac{v_j^i + v_{j-1}^i}{2}\right)\right] - h_j\left[2\left(\frac{u_j^i + u_{j-1}^i}{2}\right)^2\right]$$

$$+ h_j M_{\exp}\left[\varepsilon - \left(\frac{u_j^i + u_{j-1}^i}{2}\right)\right] + 2h_j\varepsilon^2 = 0,$$

$$\Pr{}_N\left(p_j^i - p_{j-1}^i\right) + h_j\left[\left(\frac{f_j^i + f_{j-1}^i}{2}\right)\left(\frac{p_j^i + p_{j-1}^i}{2}\right)\right] - h_j\left[\left(\frac{u_j^i + u_{j-1}^i}{2}\right)\left(\frac{g_j^i + g_{j-1}^i}{2}\right)\right]$$

$$+ h_j Nb\left[\left(\frac{s_j^i + s_{j-1}^i}{2}\right)\left(\frac{p_j^i + p_{j-1}^i}{2}\right)\right] + h_j Nt\left[\left(\frac{p_j^i + p_{j-1}^i}{2}\right)^2\right] = 0,$$

$$s_j^i - s_{j-1}^i + h_j Le\left[\left(\frac{f_j^i + f_{j-1}^i}{2}\right)\left(\frac{s_j^i + s_{j-1}^i}{2}\right) - \left(\frac{u_j^i + u_{j-1}^i}{2}\right)\left(\frac{q_j^i + q_{j-1}^i}{2}\right)\right]$$

$$+ Nt_b\left(p_j^i - p_{j-1}^i\right) = 0. \tag{27}$$

For the Newton's method, the following iterates are introduced to linearize the nonlinear system of Eqs. (27);

$$f_j^{(k+1)} = f_j^k + \delta f_j^k, \quad u_j^{(k+1)} = u_j^k + \delta u_j^k, \quad v_j^{(k+1)} = v_j^k + \delta v_j^k,$$

$$g_j^{(k+1)} = g_j^k + \delta g_j^k, \quad p_j^{(k+1)} = p_j^k + \delta p_j^k, \quad q_j^{(k+1)} = q_j^k + \delta q_j^k, \tag{28}$$

$$s_j^{(k+1)} = s_j^k + \delta s_j^k.$$

Substituting these expressions (28) into Eqs. (27), and after dropping the quadratic and higher-order terms in $\delta f_j^{(k)}$, $\delta u_j^{(k)}$, $\delta v_j^{(k)}$, $\delta g_j^{(k)}$, $\delta p_j^{(k)}$, $\delta q_j^{(k)}$ and $\delta s_j^{(k)}$ as well as the superscript i for simplicity, this procedure yields the following linear tridiagonal system;

$$\delta f_j - \delta f_{j-1} - \frac{h_j}{2}\left(\delta u_j - \delta u_{j-1}\right) = (r_1)_{j-1/2}, \ \delta u_j - \delta u_{j-1} - \frac{h_j}{2}\left(\delta v_j - \delta v_{j-1}\right) = (r_2)_{j-1/2},$$

$$\delta g_j - \delta g_{j-1} - \frac{h_j}{2}\left(\delta p_j - \delta p_{j-1}\right) = (r_3)_{j-1/2}, \ \delta q_j - \delta q_{j-1} - \frac{h_j}{2}\left(\delta s_j - \delta s_{j-1}\right) = (r_4)_{j-1/2},$$

$$(a_1)_j \delta v_j + (a_2)_j \delta v_{j-1} + (a_3)_j \delta f_j + (a_4)_j \delta f_{j-1}$$

$$+ (a_5)_j \delta u_j + (a_6)_j \delta u_{j-1} = (r_5)_{j-1/2},$$

(29)

$$(b_1)_j \delta p_j + (b_2)_j \delta p_{j-1} + (b_3)_j \delta f_j + (b_4)_j \delta f_{j-1} + (b_5)_j \delta u_j + (b_6)_j \delta u_{j-1}$$

$$+ (b_7)_j \delta g_j + (b_8)_j \delta g_{j-1} + (b_9)_j \delta s_j + (b_{10})_j \delta s_{j-1} = (r_6)_{j-1/2},$$

$$(c_1)_j \delta s_j + (c_2)_j \delta s_{j-1} + (c_3)_j \delta f_j + (c_4)_j \delta f_{j-1} + (c_5)_j \delta u_j + (c_6)_j \delta u_{j-1}$$

$$+ (c_7)_j \delta p_j + (c_8)_j \delta p_{j-1} + (c_9)_j \delta q_j + (c_{10})_j \delta q_{j-1} = (r_7)_{j-1/2},$$

where

$$(a_1)_j = 1 + \frac{h_j}{2} f_{j-1/2}, \ (a_2)_j = (a_1)_j - 2, \ (a_3)_j = \frac{h_j}{2} v_{j-1/2},$$

$$(a_4)_j = (a_3)_j, \ (a_5)_j = -2h_j u_{j-1/2} - \frac{h_j M_{\exp}}{2}, \ (a_6)_j = (a_5)_j,$$

$$(b_1)_j = 1 + \frac{h_j}{2\Pr_N} f_{j-1/2} + \frac{h_j Nb}{2\Pr_N} s_{j-1/2} + \frac{h_j Nt}{\Pr_N} p_{j-1/2}, \ (b_2)_j = (b_1)_j - 2,$$

$$(b_3)_j = \frac{h_j}{2\Pr_N} p_{j-1/2}, \ (b_4)_j = (b_3)_j, \ (b_5)_j = -\frac{h_j}{2\Pr_N} g_{j-1/2}, \ (b_6)_j = (b_5)_j,$$

$$(b_7)_j = -\frac{h_j}{2\Pr_N} u_{j-1/2}, \ (b_8)_j = (b_7)_j, \ (b_9)_j = \frac{h_j Nb}{2\Pr_N} p_{j-1/2}, \ (b_{10})_j = (b_9)_j,$$

$$(c_1)_j = 1 + \frac{h_j Le}{2} f_{j-1/2}, \ (c_2)_j = (c_1)_j - 2, \ (c_3)_j = \frac{h_j Le}{2} s_{j-1/2}, \ (c_4)_j = (c_3)_j,$$

$$(c_5)_j = -\frac{h_j Le}{2} q_{j-1/2}, \ (c_6)_j = (c_5)_j, \ (c_7)_j = Nt_b, \ (c_8)_j = -Nt_b,$$

$$(c_9)_j = -\frac{h_j Le}{2} u_{j-1/2}, \ (c_{10})_j = (c_9)_j,$$

$$\left(r_1\right)_{j-1/2} = f_{j-1} - f_{j-1} + h_j u_{j-1/2}, \left(r_2\right)_{j-1/2} = u_{j-1} - u_{j-1} + h_j v_{j-1/2},$$

$$\left(r_3\right)_{j-1/2} = g_{j-1} - g_{j-1} + h_j p_{j-1/2}, \left(r_4\right)_{j-1/2} = q_{j-1} - q_{j-1} + h_j s_{j-1/2},$$

$$\left(r_5\right)_{j-1/2} = \left(v_{j-1} - v_j\right) - h_j f_{j-1/2} v_{j-1/2} + 2h_j u_{j-1/2}^2 + h_j M_{\exp} u_{j-1/2}$$
$$- 2h_j \varepsilon^2 - h_j M_{\exp}\varepsilon,$$

$$\left(r_6\right)_{j-1/2} = p_{j-1} - p_j - h_j\left(\frac{1}{Pr_N}\right) f_{j-1/2} p_{j-1/2} + h_j\left(\frac{1}{Pr_N}\right) u_{j-1/2} g_{j-1/2}$$

$$- h_j Nt\left(\frac{1}{Pr_N}\right) p_{j-1/2}^2 - h_j Nb\left(\frac{1}{Pr_N}\right) s_{j-1/2} p_{j-1/2},$$

$$\left(r_7\right)_{j-1/2} = s_{j-1} - s_j - h_j Le\left(f_{j-1/2} s_{j-1/2} - u_{j-1/2} q_{j-1/2}\right) + Nt_b\left(p_{j-1} - p_j\right).$$

To complete the system (22), the boundary conditions (19) are recalled that can be satisfied exactly with no iteration [25]. So, the correct values in all the iterations are maintained by taking;

$$\delta f_0 = 0, \ \delta u_0 = 0, \ \delta h_0 = 0, \ \delta g_0 = 0, \ \delta q_0 = 0,$$
$$\delta u_J = 0, \ \delta h_0 = 0, \ \delta g_J = 0, \ \delta q_J = 0. \tag{30}$$

The Block-elimination method

The linearized differential equations of the system (29) have a block-tridiagonal structure. In vector-matrix form, it can be written as;

$$[A][\delta] = [r], \tag{31}$$

where

$$[A] = \begin{bmatrix} [A_1] & [C_1] & & & & \\ [B_2] & [A_2] & [C_2] & & & \\ & & \ddots & & & \\ & & & \ddots & & \\ & & & & \ddots & \\ & & & [B_{J-1}] & [A_{J-1}] & [C_{J-1}] \\ & & & & [B_J] & [C_J] \end{bmatrix}, [\delta] = \begin{bmatrix} [\delta_1] \\ [\delta_2] \\ \vdots \\ [\delta_{J-1}] \\ [\delta_J] \end{bmatrix}, [r] = \begin{bmatrix} [r_1] \\ [r_2] \\ \vdots \\ [r_{J-1}] \\ [r_J] \end{bmatrix}. \tag{32}$$

The block-tridiagonal structure commonly consists of variables or constants, but here, an interesting feature can be observed that is, for the Keller's Box method, it consists of block matrices. By taking $e_j = -\dfrac{h_j}{2}$, the elements of matrices are defined as follows;

$$[A_1] = \begin{bmatrix} 0 & 0 & 0 & 1 & 0 & 0 & 0 \\ e_1 & 0 & 0 & 0 & e_1 & 0 & 0 \\ 0 & e_1 & 0 & 0 & 0 & e_1 & 0 \\ 0 & 0 & e_1 & 0 & 0 & 0 & e_1 \\ (a_2)_1 & 0 & 0 & (a_3)_1 & (a_1)_1 & 0 & 0 \\ 0 & (b_2)_1 & (b_{10})_1 & (b_3)_1 & 0 & (b_1)_1 & (b_9)_1 \\ 0 & (c_8)_1 & (c_2)_1 & (c_3)_1 & 0 & (c_7)_1 & (c_1)_1 \end{bmatrix}, \tag{33}$$

$$[A_j] = \begin{bmatrix} e_j & 0 & 0 & 1 & 0 & 0 & 0 \\ -1 & 0 & 0 & 0 & e_j & 0 & 0 \\ 0 & -1 & 0 & 0 & 0 & e_j & 0 \\ 0 & 0 & -1 & 0 & 0 & 0 & e_j \\ (a_6)_j & 0 & 0 & (a_3)_j & (a_1)_j & 0 & 0 \\ (b_6)_j & (b_8)_j & 0 & (b_3)_j & 0 & (b_1)_j & (b_9)_j \\ (c_6)_j & 0 & (c_{10})_j & (c_3)_j & 0 & (c_7)_j & (c_1)_j \end{bmatrix}, \; 2 \le j \le J, \tag{34}$$

$$[B_j] = \begin{bmatrix} 0 & 0 & 0 & -1 & 0 & 0 & 0 \\ 0 & 0 & 0 & 0 & e_j & 0 & 0 \\ 0 & 0 & 0 & 0 & 0 & e_j & 0 \\ 0 & 0 & 0 & 0 & 0 & 0 & e_j \\ 0 & 0 & 0 & (a_4)_j & (a_2)_j & 0 & 0 \\ 0 & 0 & 0 & (b_4)_j & 0 & (b_2)_j & (b_{10})_j \\ 0 & 0 & 0 & (c_4)_j & 0 & (c_8)_j & (c_2)_j \end{bmatrix}, \; 2 \le j \le J, \tag{35}$$

$$
[C_j] = \begin{bmatrix}
e_j & 0 & 0 & 0 & 0 & 0 & 0 \\
1 & 0 & 0 & 0 & 0 & 0 & 0 \\
0 & 1 & 0 & 0 & 0 & 0 & 0 \\
0 & 0 & 1 & 0 & 0 & 0 & 0 \\
(a_5)_j & 0 & 0 & 0 & 0 & 0 & 0 \\
(b_5)_j & (b_7)_j & 0 & 0 & 0 & 0 & 0 \\
(c_5)_j & 0 & (c_9)_j & 0 & 0 & 0 & 0
\end{bmatrix}, \quad 1 \le j \le J-1,
\tag{36}
$$

$$
[\delta_1] = \begin{bmatrix}
\delta v_0 \\
\delta p_0 \\
\delta s_0 \\
\delta f_1 \\
\delta v_1 \\
\delta p_1 \\
\delta s_1
\end{bmatrix}, \qquad
[\delta_j] = \begin{bmatrix}
\delta u_{j-1} \\
\delta g_{j-1} \\
\delta q_{j-1} \\
\delta f_j \\
\delta v_j \\
\delta p_j \\
\delta s_j
\end{bmatrix}, \quad 2 \le j \le J,
\tag{37}
$$

and

$$
[r_j] = \begin{bmatrix}
(r_1)_{j-1/2} \\
(r_2)_{j-1/2} \\
(r_3)_{j-1/2} \\
(r_4)_{j-1/2} \\
(r_5)_{j-1/2} \\
(r_6)_{j-1/2} \\
(r_7)_{j-1/2}
\end{bmatrix}, \qquad 1 \le j \le J.
\tag{38}
$$

The coefficient matrix A is known as a tridiagonal matrix due to the fact that all elements of $[A]$ are zero except those 3 along the diagonal. To solve Eq. (31), $[A]$ is assumed to be nonsingular and can be factorized into;

$$
[A] = [L][U],
\tag{39}
$$

where

$$
[L] = \begin{bmatrix}
[I] & & & & & \\
[\Gamma_2] & [I] & & & & \\
& & \ddots & & & \\
& & & \ddots & & \\
& & & & [I] & \\
& & & & [\Gamma_J] & [I]
\end{bmatrix}, \text{ and } [U] = \begin{bmatrix}
[\alpha_1] & [C_1] & & & \\
& [\alpha_2] & [C_2] & & \\
& & \ddots & & \\
& & & \ddots & \\
& & & [\alpha_{J-1}] & [C_{J-1}] \\
& & & & [\alpha_J]
\end{bmatrix}, \tag{40}
$$

where $[I]$ is the identity matrix of order 7 and $[\alpha_i]$, $[\Gamma_i]$ are 7×7 matrices whose elements are determined by the following equations;

$$
[\alpha_1] = [A_1], \tag{41}
$$

$$
[A_1][\Gamma_1] = [C_1], \tag{42}
$$

and

$$
[\alpha_j] = [A_j] - [B_j][\Gamma_{j-1}], \qquad j = 2, 3, \dots\dots, J, \tag{43}
$$

$$
[\alpha_j][\Gamma_j] = [C_j], \qquad j = 2, 3, \dots\dots, J. \tag{44}
$$

Eq. (39) can be substituted into Eq. (31), which is;

$$
[L][U][\delta] = [r]. \tag{45}
$$

if

$$
[U][\delta] = [W], \tag{46}
$$

then Eq. (45) becomes;

$$
[L][W] = [r], \tag{47}
$$

where

$$
[W] = \begin{bmatrix}
[W_1] \\
[W_2] \\
\vdots \\
[W_{J-1}] \\
[W_J]
\end{bmatrix}, \tag{48}
$$

here $[W_j]$ are 7×1 column matrices. The elements $[W]$ can be solved from Eq. (47);

$$
[\alpha_1][W_1] = [r_1], \tag{49}
$$

$$
[\alpha_j][W_j] = [r_j] - [B_j][W_{j-1}], \qquad 2 \le j \le J. \tag{50}
$$

The step in which $[\Gamma_j]$, $[\alpha_j]$ and $[W_j]$ are calculated is usually referred to as the forward sweep. Once the elements of $[W]$ are found, Eq. (47) then gives the solution $[\delta]$ in the so-called backward sweep, in which the elements are obtained by the following relations;

$$[\delta_J] = [W_J],\tag{51}$$

$$[\delta_j] = [W_j] - [\Gamma_j][\delta_{j+1}], \quad 2 \le j \le J.\tag{52}$$

Once the elements of $[\delta]$ are found, Eqs. (29) can be used to find the $(k+1)$th iteration in Eq. (27).

Starting conditions

Keller-box method is unique in which various spacing along x and y directions can be used. For the numerical computation, a proper step size and appropriate value of the boundary layer thickness must be determined. In general, computation can be started by using a small value of η_∞ and then successively increase it until a suitable value is obtained. In some cases, too small or too large values of η_∞ may give rise to the convergence problem. For most laminar boundary layer flows, the transformed boundary layer thickness (η) is almost constant [25] and typically lies between 5 and 10. In order to start and proceed with the numerical computation, it is necessary to make initial guesses for the functions f, u, v, g, p, q, and s across the boundary layer from $\eta = 0$ to $\eta \to \infty$. There are few checks on the selections of distribution curves that they must satisfy the boundary conditions (15). Different guesses of the initial value profiles will give the same final result but the iteration counts and the computation time may be more or less. For the present problem, the following initial value profiles have been taken;

$$f(\eta) = \eta + \left(\frac{\eta^2}{2\eta_\infty}\right)(\varepsilon - 1), \; f'(\eta) = u(\eta) = 1 + \left(\frac{\eta}{\eta_\infty}\right)(\varepsilon - 1), \; f''(\eta) = v(\eta) = \left(\frac{1}{\eta_\infty}\right)(\varepsilon - 1),$$

$$\theta(\eta) = g(\eta) = 1 - \frac{\eta}{\eta_\infty}, \; \theta'(\eta) = p(\eta) = \frac{1}{\eta_\infty}, \; \phi(\eta) = q(\eta) = 1 - \frac{\eta}{\eta_\infty}, \; \phi'(\eta) = s(\eta) = -\frac{1}{\eta_\infty}.\tag{53}$$

In the laminar flow calculations, the wall shear stress parameter $v(\eta)$ is commonly used as the convergence criterion where iterations are repeated until the convergence is satisfied. Therefore, calculations are stopped when;

$$\left| \delta v_0^{(i)} \right| < \varepsilon_1,\tag{54}$$

where ε_1 is a small prescribed value $(\varepsilon_1 = 0.00001)$ which shows the accuracy of most predicted quantities up to 4 decimal places [25].

Results and discussion

The coupled nonlinear ordinary differential Eqs. (11) - (13) subjected to the boundary conditions (15) are solved numerically by using the finite difference scheme known as the Keller-box method. The numerical results for physical parameters of interest such as Brownian motion parameter Nb, thermophoresis parameter Nt, velocity ratio parameter ε, radiation parameter N, Prandtl number Pr, Lewis number Le and Hartmann number $M_{\exp}$ are given in Tabular form (**Tables 1** and **2**) and displayed graphically (**Figures 3 - 13**). **Table 1** shows a comparison of obtained results for the reduced Nusselt number $-\theta'(0)$ with the results given by [19,20]. These comparisons show an excellent agreement between the obtained numerical results and existing results in the literature.

Table 1 Comparison of the reduced Nusselt number $-\theta'(0)$ when $Nb = Nt = Le = \varepsilon = 0$.

Pr	M_{exp}	N	[19] $-\theta'(0)$	[20] $-\theta'(0)$	**Present results** $-\theta'(0)$
1	0	0	0.9548	0.9548	0.9548
2	0	0	1.4714	1.4714	1.4714
3	0	0	1.8691	1.8691	1.8691
1	0	1.0	0.5315	0.5312	0.5312
1	1.0	0	-	0.8611	0.8611
1	1.0	1.0	-	0.4505	0.4505

Table 2 shows the variations of the reduced Nusselt number $-\theta'(0)$, the reduced Sherwood number $-\phi'(0)$ and the skin-friction coefficient $C_{fx}(0)$ for different values of Nb, Nt, Pr, Le, M_{exp}, N and ε. It is observed form this table that $-\theta'(0)$ decreases with the increasing values of Nb, Nt, Le and N whereas it increases for increasing values of Pr and ε. These decreasing effects in $-\theta'(0)$ with respect to Nb and Nt play an important role for the deeper penetration into the fluid which acts as a good thickener for the thermal boundary layer. It is due to the fact that the presence of the nanoparticles in the base fluid increases the effective thermal conductivity of the fluid significantly and as a result enhances the heat transfer characteristics of the nanofluid. However, it is found that $-\phi'(0)$ decreases for the increasing values of Nt and Pr whereas it increases for increasing values of Nb, Le, ε and N. Further, it is observed that $C_{fx}(0)$ decreases for increasing values of ε. Here, it is noted that for the increasing values of M_{exp}, $-\theta'(0)$, $-\phi'(0)$ and $C_{fx}(0)$ show a quite opposite effect in both cases of $\varepsilon < 1$ and $\varepsilon > 1$. The values of $C_{fx}(0)$ are found to be positive when $\varepsilon < 1$, which means that nanofluids exert a drag force on the solid boundary while negative values of $C_{fx}(0)$ show an opposite effect when $\varepsilon > 1$.

Table 2 Values of the reduced Nusselt number $-\theta'(0)$, the reduced Sherwood number $-\phi'(0)$ and the skin-friction coefficient $C_{fx}(0)$.

Nb	*Nt*	**Pr**	*Le*	M_{exp}	ε	N	$-\theta'(0)$	$-\phi'(0)$	$C_{fx}(0)$
0.1	0.1	1.00	10	0.1	0.1	1.0	0.5382	3.5382	1.2856
0.5	0.1	1.00	10	0.1	0.1	1.0	0.4710	3.6457	1.2856
0.1	**0.5**	1.00	10	0.1	0.1	1.0	0.5094	3.0958	1.2856
0.1	0.1	**10.0**	10	0.1	0.1	1.0	1.6472	3.1073	1.2856
0.1	0.1	1.00	**25**	0.1	0.1	1.0	0.5363	5.8844	1.2856
0.1	0.1	1.00	10	**2.5**	0.1	1.0	0.4690	3.3924	1.8977
0.1	0.1	1.00	10	2.5	**1.1**	1.0	0.8078	3.8964	-0.2702
0.1	0.1	1.00	10	0.1	**0.9**	1.0	0.7581	3.8017	0.2083
0.1	0.1	1.00	10	0.1	**1.1**	1.0	0.8028	3.8880	-0.2216
0.1	0.1	1.00	10	0.1	**2.0**	1.0	0.9796	4.2732	-2.7348
0.1	0.1	1.00	10	0.1	0.1	**3.0**	0.3361	3.5984	1.2856

Figure 3 shows the effects of M_{exp} and ε on the velocity profiles $f'(\eta)$ for fixed values of *Nb*, *Nt*, Pr, *Le* and N when $\varepsilon < 1$, $\varepsilon = 1$ and $\varepsilon > 1$. This figure shows that $f'(\eta)$ decreases for increasing values of M_{exp} for the case of $\varepsilon < 1$. Here, the decreasing behavior in $f'(\eta)$ is justified due to the fact that larger values of M_{exp} increase the resistive forces on the stretching surface which result in a retardation force to slow down the nanofluid motions. However, in the case of $\varepsilon > 1$, $f'(\eta)$ increases for the increasing values of M_{exp}. It is further observed that $f'(\eta)$ increases for increasing values of ε. It is interesting to note that in the case of $\varepsilon > 1$, the momentum boundary layer thickness becomes smaller compared to the case of $\varepsilon < 1$ and causes an inverted boundary layer structure. Moreover, when $\varepsilon = 1$, $f'(\eta)$ coincide with each other and results in a degenerate inviscid flow, where the stretching matches the conditions at infinity. This means that in the case when the external stream velocity becomes equal to the stretching velocity, the flow field is not influenced by the different values of the incorporated flow parameters.
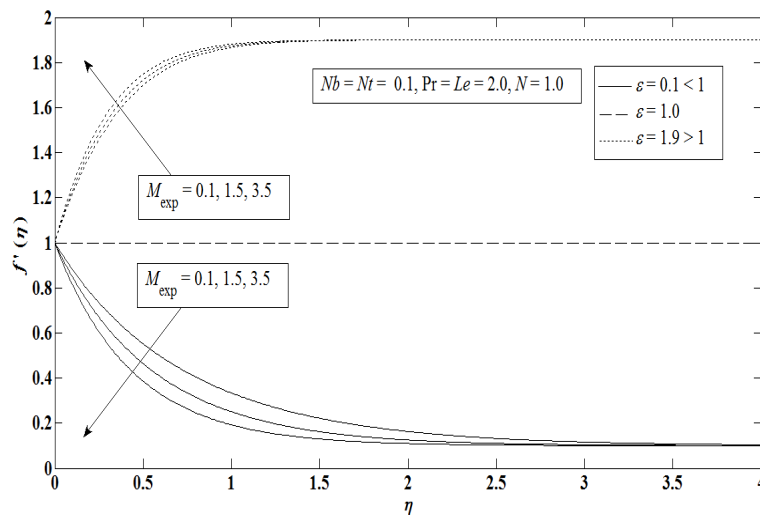
Figure 3 Velocity profiles against η for different values of M_{exp}.

Temperature profiles $\theta(\eta)$ for both cases of $\varepsilon < 1$ and $\varepsilon > 1$ are shown in **Figures 4 - 8**, respectively. It is observed from **Figures 4 - 7** that $\theta(\eta)$ increases for the increasing values of Nb, Nt and N whereas it decreases for increasing values of Pr. This decrease in $\theta(\eta)$ with an increase in Pr is significant due to the fact that Pr increases in 2 ways either by increasing the size of the nanoparticles or by increasing the viscosity of the base fluid which causes a decrease in the conduction phenomenon to shorten the thermal boundary layer thickness and the heat transfer is found to be smaller for larger values of Pr. In contrast, increasing values of N show a substantial increase in the thermal conductivity of the nanofluid and hence $\theta(\eta)$ increases for increasing values of N [19]. **Figure 8** shows that $\theta(\eta)$ increases with increasing values of M_{exp} when $\varepsilon < 1$ while it decreases in the case of $\varepsilon > 1$. From this figure, it is noticed that the thermal boundary layer thickness is not much influenced by the larger values of M_{exp} when $\varepsilon > 1$.
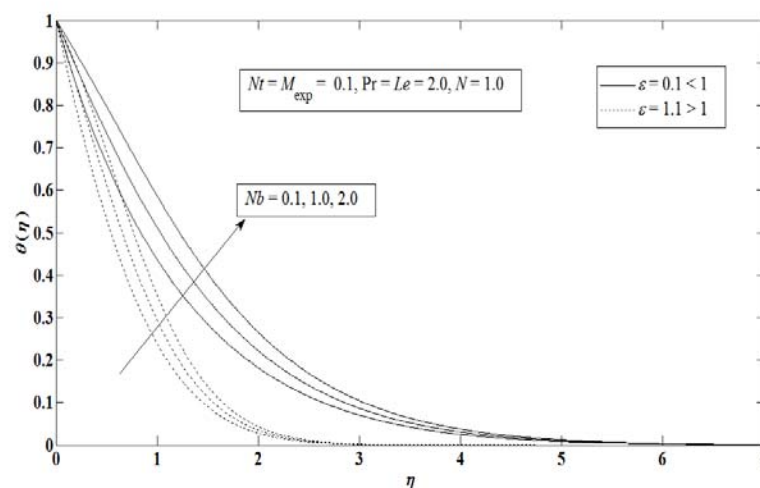
Figure 4 Temperature profiles against η for different values of Nb.
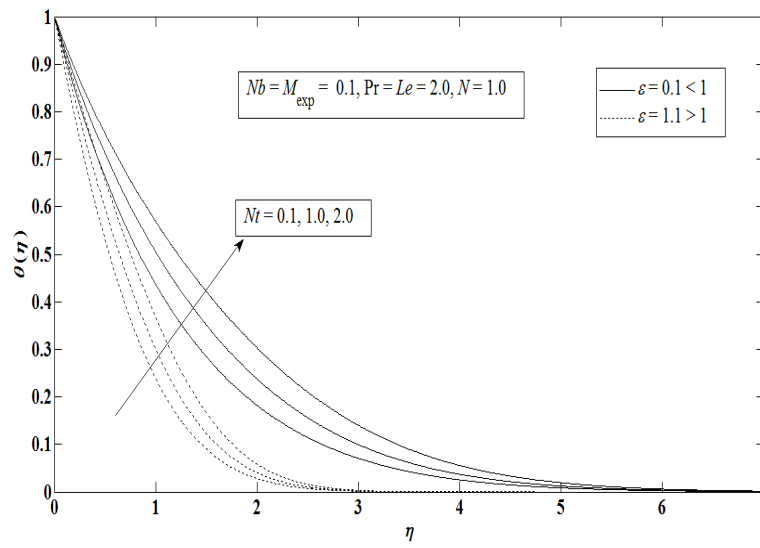
Figure 5 Temperature profiles against η for different values of Nt.
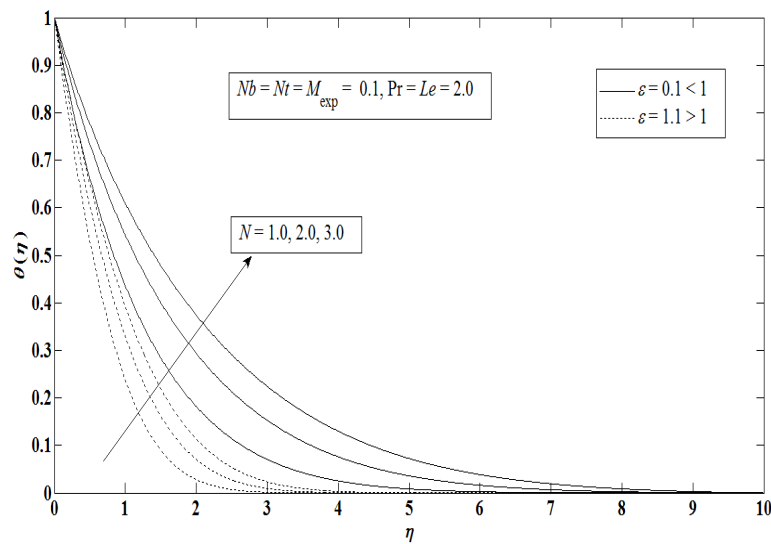
Figure 6 Temperature profiles against η for different values of N.
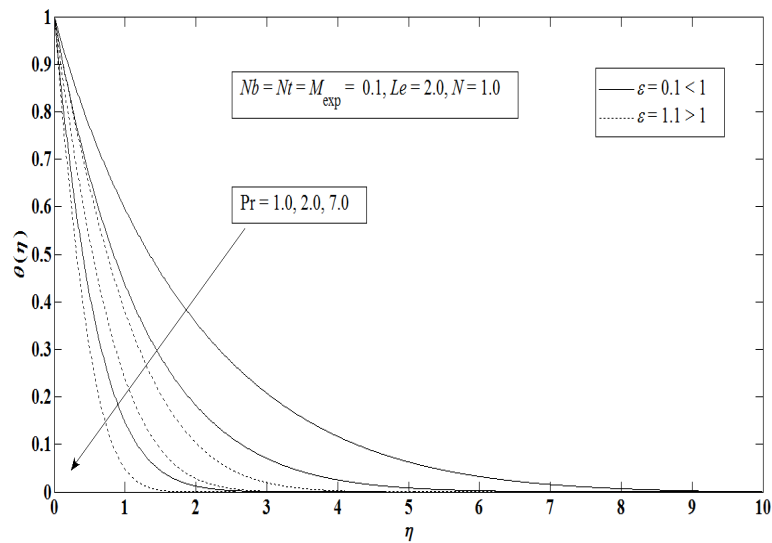
Figure 7 Temperature profiles against η for different values of Pr.
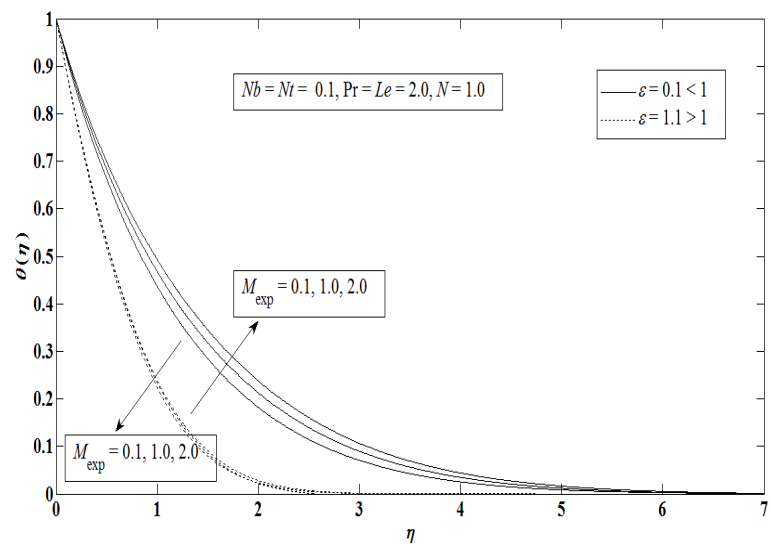
Figure 8 Temperature profiles against η for different values of $M_{\exp}$.

Figures 9 - 13 are prepared to study the effects of different embedded flow parameters on concentration profiles $\phi(\eta)$. **Figures 9 - 12** show that $\phi(\eta)$ decreases with increasing values of Nb, Le and N whereas it increases for increasing values of Nt. **Figure 13** illustrates that for the increasing values of $M_{\exp}$, $\phi(\eta)$ increases when $\varepsilon < 1$ while it decreases when $\varepsilon > 1$. Here, it is important to note that the increasing values of $M_{\exp}$ shows minimal changes in $\theta(\eta)$ and $\phi(\eta)$ (**Figures 8** and **13**). In addition, the above discussed figures show that the momentum, thermal and concentration boundary layer thicknesses are greater when $\varepsilon < 1$ compared to $\varepsilon > 1$.
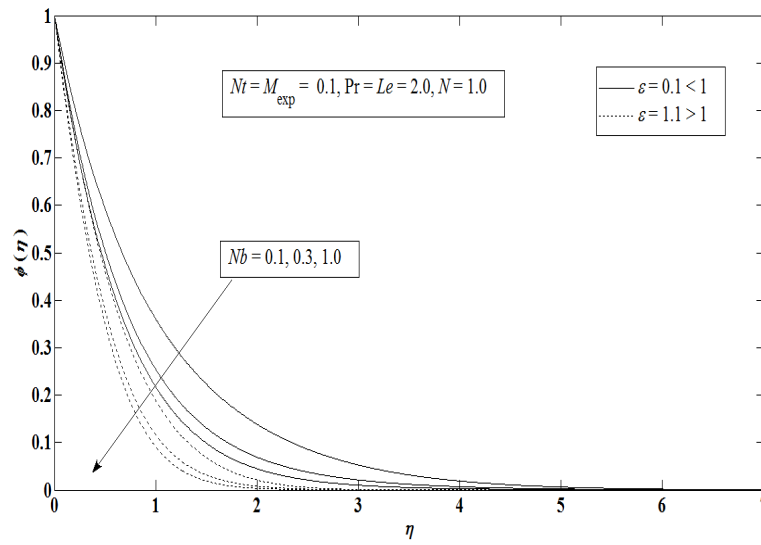
Figure 9 Concentration profiles against η for different values of *Nb*.
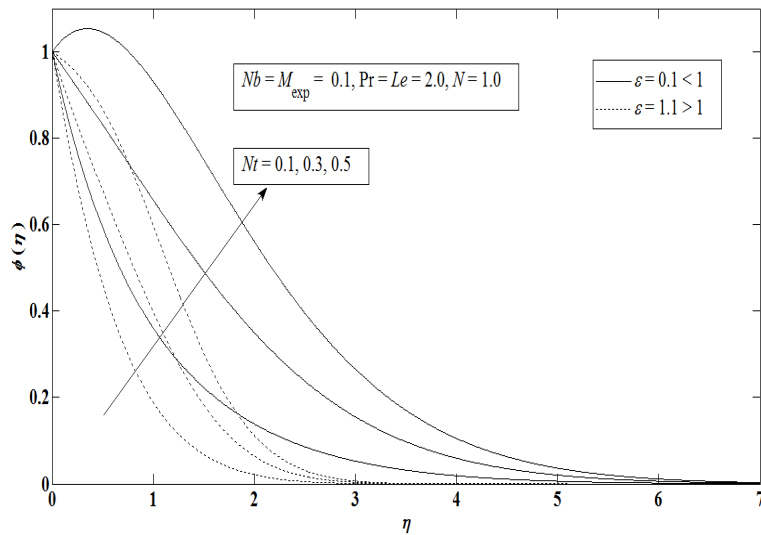
Figure 10 Concentration profiles against η for different values of *Nt*.
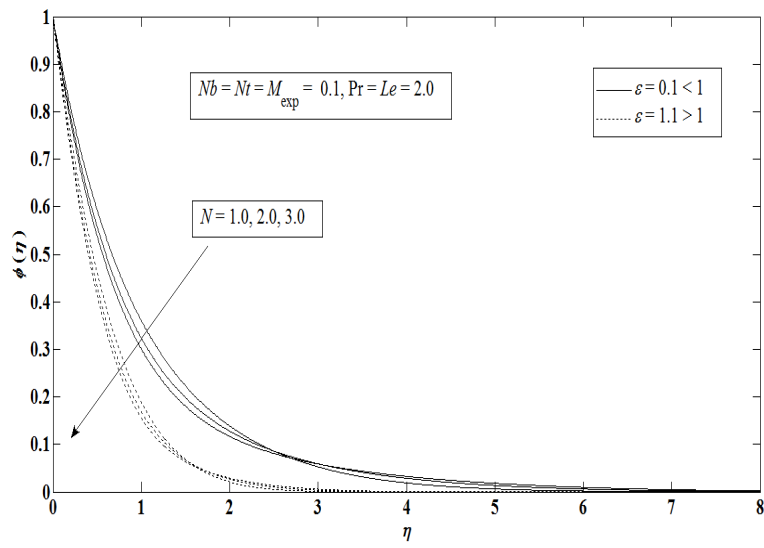
Figure 11 Concentration profiles against η for different values of *N*.
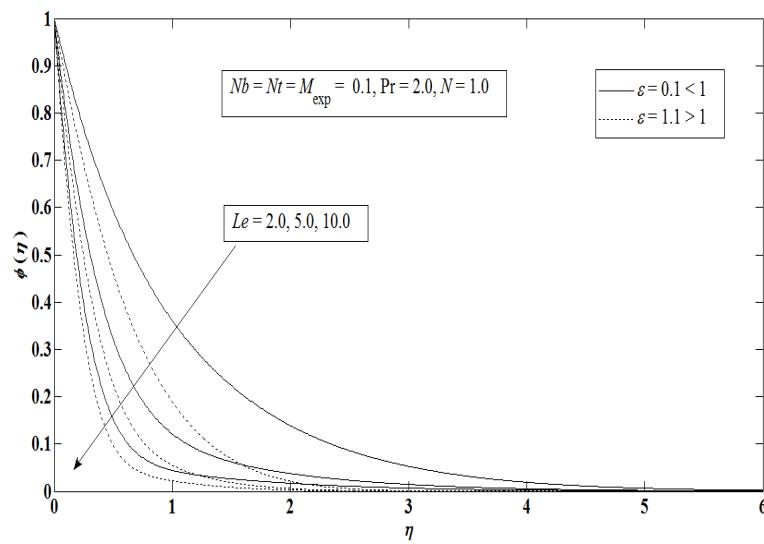
Figure 12 Concentration profiles against η for different values of *Le*.
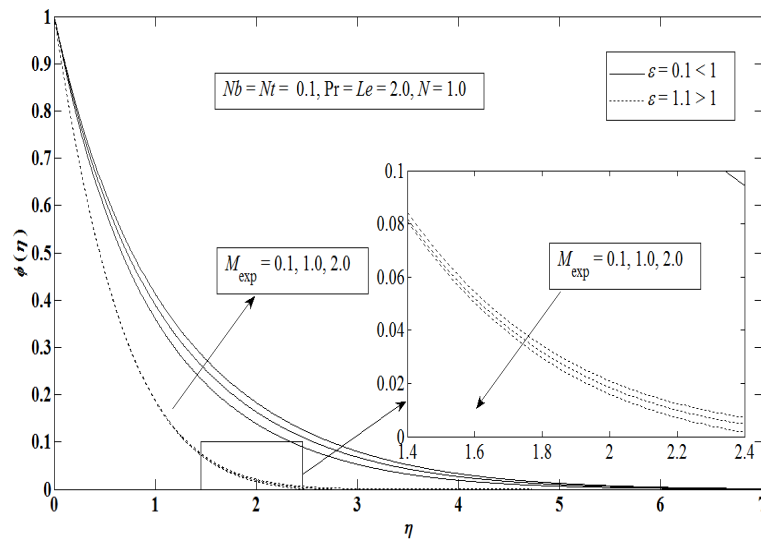
Figure 13 Concentration profiles against η for different values of $M_{\exp}$.

Conclusions

In the present article the radiation effect on MHD stagnation-point flow of a nanofluid over an exponentially stretching sheet is investigated. The governing nonlinear partial differential equations are solved numerically by using the Keller-box method. An analysis is made through the graphical and tabulated data for the flow of heat and mass transfer in the nanofluid when the free stream velocity is equal, greater and less than the stretching velocity. This study reveals the following trends;

1) The velocity profiles coincide with each other if $\varepsilon = 1$ and results in a degenerate inviscid flow where the stretching matches the conditions at infinity.

2) The external stream velocity increases compared to the stretching velocity and the momentum boundary layer thickness shortens when $\varepsilon > 1$ whereas an inverted boundary layer structure is found when $\varepsilon < 1$.

3) Increasing values of $M_{\exp}$ has a minimal influence on the momentum, thermal and concentration boundary layers in the case when $\varepsilon > 1$.

Acknowledgements

References

[1] K Hiemenz. Die Grenzschicht an einem in den gleichförmigen Flüssigkeitsstrom eingetauchten geraden Kreiszylinder. *Dingler's Polytech. J.* 1911; **326**, 321-4.

[2] TR Mahapatra and AS Gupta. Heat transfer in stagnation-point flow towards a stretching sheet. *Heat Mass Tran.* 2002; **38**, 517-21.

[3] TR Mahapatra and AS Gupta. Stagnation-point flow towards a stretching surface. *Can. J. Chem. Eng.* 2003; **81**, 258-63.

[4] R Nazar, N Amin, D Filip and I Pop. Stagnation point flow of a micropolar fluid towards a stretching sheet. *Int. J. Nonlinear Mech.* 2004; **39**, 1227-35.

[5] YY Lok, N Amin and I Pop. Non-orthogonal stagnation point flow towards a stretching sheet. *Int. J.*

Nonlinear Mech. 2006; **41**, 622-7.

[6] S Nadeem, A Hussain, MY Malik and T Hayat. Series solutions for the stagnation flow of a second-grade fluid over a shrinking sheet. *Appl. Math. Mech. Eng. Ed*. 2009; **30**, 1255-62.

[7] S Nadeem, A Hussain and M Khan. HAM solutions for boundary layer flow in the region of the stagnation point towards a stretching sheet. *Comm. Nonlinear Sci. Numer. Simulat*. 2010; **15**, 475-81.

[8] F Labropulu, D Li and I Pop. Non-orthogonal stagnation-point flow towards a stretching surface in a non-Newtonian fluid with heat transfer. *Int. J. Therm. Sci*. 2010; **49**, 1042-50.

[9] A Ishak, YY Lok and I Pop. Stagnation-point flow over a shrinking sheet in a micropolar fluid. *Chem. Eng. Comm*. 2010; **197**, 1417-27.

[10] N Bachok, A Ishak and I Pop. Boundary-layer flow of nanofluid over a moving surface in a flowing fluid. *Int. J. Therm. Sci*. 2010; **49**, 1663-8.

[11] M Patel and MG Timol. Orthogonal stagnation point flow of a power law fluid towards a stretching surface. *Int. J. Appl. Math. Mech*. 2011; **7**, 31-7.

[12] N Bachok, A Ishak and I Pop. On the stagnation point flow towards a stretching sheet with homogeneous-heterogeneous reactions effects. *Comm. Nonlinear Sci. Numer. Simulat*. 2011; **16**, 4296-302.

[13] AV Kuznetsov and DA Nield. Natural convective boundary-layer flow of a nanofluid past a vertical plate. *Int. J. Therm. Sci*. 2010; **49**, 243-7.

[14] N Bachok, A Ishak and I Pop. Melting heat transfer in boundary layer stagnation-point flow towards a stretching/shrinking sheet. *Phys. Lett. A* 2010; **374**, 4075-9.

[15] N Bachok, A Ishak and I Pop. Boundary layer stagnation-point flow and heat transfer over an exponentially stretching/shrinking sheet in a nanofluid. *Int. J. Heat Mass Tran*. 2012; **55**, 8122-8.

[16] M Ashraf and M Rashid. MHD boundary layer stagnation point flow and heat transfer of a micropolar fluid towards a heated shrinking sheet with radiation and heat generation. *World Appl. Sci. J*. 2012; **16**, 1338-51.

[17] AA Afify and NS Elgazery. Lie group analysis for the effects of chemical reaction on MHD stagnation-point flow of heat and mass transfer towards a heated porous stretching sheet with suction or injection. *Nonlinear Anal. Model. Contr*. 2012; **17**, 1-15.

[18] M Ferdows, MS Khan, MM Alam and S Sun. MHD mixed convective boundary layer flow of a nanofluid through a porous medium due to an exponentially stretching sheet. *Math. Prob. Eng*. 2012; **2012**, Article ID 408528.

[19] B Bidin and R Nazar. Numerical solution of the boundary layer flow over an exponentially stretching sheet with thermal radiation. *Eur. J. Sci. Res*. 2009; **33**, 710-7.

[20] A Ishak. MHD boundary layer flow due to an exponentially stretching sheet with radiation effect. *Sains Malays*. 2011; **40**, 391-5.

[21] Y Ding, H Chen, L Wang, CY Yang, Y He, W Yang, WP Lee, L Zhang and R Huo. Heat transfer intensification using nanofluids. *Kona* 2007; **25**, 23-38.

[22] CH Chen. Effects of magnetic field and suction or injection on convection heat transfer of non-Newtonian power law fluids past a power law stretched sheet with surface seat slux. *Int. J. Therm. Sci*. 2008; **47**, 954-61.

[23] RD Cess. The interaction of thermal radiation with free convection heat transfer. *Int. J. Heat Mass Tran*. 1966; **9**, 1269-77.

[24] FM Hady, FS Ibrahim, SM Abdel-Gaied and MR Eid. Radiation effect on viscous flow of a nanofluid and heat transfer over a nonlinearly stretching sheet. *Nanoscale Res. Lett*. 2012; **7**, Article ID 229.

[25] T Cebeci and P Bradshaw. *Physical and Computational Aspects of Convective Heat Transfer*. Springer-Verlag, New York, 1988.